Ocean Engineering 195 (2020) 106695

Contents lists available at ScienceDirect

Ocean Engineering

journal homepage: www.elsevier.com/locate/oceaneng

# Formation and estimation of peak impact force on suspended pipelines due to submarine debris flow

Xuesheng Qian [a,b,*], Jingping Xu [a], Yong Bai [c], Himangshu S. Das [d]

[a] Department of Ocean Science and Engineering, Southern University of Science and Technology, Shenzhen, Guangdong, China
[b] School of Civil Engineering, Southeast University, Nanjing, Jiangsu, China
[c] College of Civil Engineering and Architecture, Zhejiang University, Hangzhou, Zhejiang, China
[d] Engineering and Construction Division, US Army Corps of Engineers, Galveston, TX, USA

ARTICLE INFO

*Keywords:*
Suspended pipeline
Submarine debris flow
Constant impact velocity
Peak impact force
Inertia coefficient
Local acceleration

ABSTRACT

In recent years, submarine debris-flow impact on suspended pipeline has been extensively investigated. Typical modes of impact force are identified: At low Reynolds number, it increases till reaches a stable plateau; otherwise, it sharply rises to a peak before decreasing to a stable value. However, the formation mechanism of peak impact force remains an open question. To address this issue, a two-dimensional (2D) biphasic (slurry and water) numerical model is developed using ANSYS Fluent 18.0. This model is used to simulate the constant-speed submarine debris-flow impact on a suspended pipeline. Herein, similar modes of peak and stable impact coefficients, which are nondimensionalized impact forces, on a suspended pipeline are observed. The formation mechanism of peak impact force is revealed. It is found that, the stable impact force relies on the constant speed of a submarine debris flow, while peak impact force depends on its velocity and local acceleration at initial impact. Moreover, the relationships between Reynolds number and coefficients of inertia and drag are proposed to estimate the peak and stable impact forces. The relations are compared to experimental and numerical datasets available in literatures, and laboratory experiments are recommended in future to obtain more measured datasets for further verification.

## 1. Introduction

Submarine pipelines are critical seafloor installations often deployed for efficient transportation of strategic energy and mineral resources from the offshore production fields to onshore processing and ancillary storage facilities (Kaiser, 2017). The corridors for pipeline routes are extensively surveyed and prudently selected before carrying out on-site constructions to circumvent hazardous areas with potential seafloor instabilities. Even so, they are still inevitably exposed to the devastating threats of failed soil masses due to long runout distances (White et al., 2016). The soil masses emitted from the underwater slope failures are transported typically in the form of gravity-driven sediment flows, such as debris flows and turbidity currents. Submarine debris flows are very dense non-Newtonian fluids in laminar regime, with density up to 1800 kg/m$^3$ and velocity up to 30 m/s (Drago, 2002); On the other hand, turbidity currents are dilute turbulent Newtonian flows, with density higher than ambient water and up to 1200 kg/m$^3$. Maximum velocity reached by turbidity currents is on the order of 10–15 m/s (Drago, 2002). As such, submarine debris flows contain much larger momentum with the potential for catastrophic disasters to seafloor structures, which is a major concern for engineering design of offshore structures such as submarine pipelines (Malgesini et al., 2018).

Submarine debris-flow impact forces on pipelines are rudimentary yet critical information for optimization of structural design and mitigation of hazardous effects. Evaluation methods of submarine debris-flow impact force on a pipeline are divided by two distinct approaches: soil and fluid mechanics. The soil mechanics approach was developed after failure of three platforms and associated pipelines in the northern Gulf of Mexico during the Hurricane Camille in 1969 (Zakeri, 2009a). With an empirical parameter, the impact force is assumed to be proportional to undrained shear strength of sliding mass. The empirical parameter was initially set to constant values (e.g. Demars, 1978; Bea and Aurora, 1982), and later improved with consideration of soil strain-rate effects (e.g. Shcapery and Dunlap, 1978; Zakeri et al., 2012).

* Corresponding author. Department of Ocean Science and Engineering, Southern University of Science and Technology, 1088 Xueyuan Avenue, Shenzhen, Guangdong, 518055, China.
*E-mail address:* qianxs@sustech.edu.cn (X. Qian).

https://doi.org/10.1016/j.oceaneng.2019.106695
Received 12 July 2019; Received in revised form 2 November 2019; Accepted 4 November 2019
Available online 15 November 2019

The soil mechanics approach is more applicable to early stage of failed mass, when undrained shear strength of soil is close to the intact in-situ state. However, submarine debris flows have very high fluidity, and thus the fluid mechanics approach seems to be more appropriate (Zakeri et al., 2008; Randolph et al., 2011).

In fluid mechanics approach, drag equation is widely used to estimate submarine debris-flow impact force on pipelines. In the drag equation, the impact force is proportional to the square of velocity. Though researchers (e.g. Pazwash and Robertson, 1975) began early to investigate the impact forces exerted by non-Newtonian fluid flowing around objects, evaluation of impact force on a pipeline due to submarine debris-flow impact started to be performed merely a decade ago (Zakeri et al., 2008). Zakeri et al. (2008) launched a series of flume tests to investigate submarine debris-flow impact force normally acting on a pipeline. Through lab experiments and supplemental Computational Fluid Dynamics (CFD) analyses (Zakeri et al., 2009b), they proposed empirical relations between drag coefficient and Reynolds number for suspended and as-laid pipelines. Afterwards, several researchers followed up their pioneering work to study the normal and longitudinal impact forces on suspended (Zakeri, 2009c; Liu et al., 2015) and as-laid (Wang et al., 2016) pipelines at various angles of debris-flow attack. They extended the drag coefficient as a function of Reynolds number and angle of attack. Besides, some researchers studied normal impact force on a pipeline under different suspension height (Li et al., 2015; Guo et al., 2019), and correlated drag coefficient with Reynolds number and suspension height. Other researchers studied the effects of various factors, such as the streamlined cross-section of a pipeline (Perez--Gruszkiewicz, 2012; Fan et al., 2018), low-temperature environment near seabed (Nian et al., 2018), and cavity of negative pressure formed behind a pipeline (Dutta and Hawlader, 2019), on the impact force acting on a suspended pipeline.

It should be noted that, all previous efforts are made to estimate the impact force on a pipeline imposed by a constant-speed submarine debris flow. Also, since suspended pipelines are more vulnerable to debris-flow impact than the laid-on-seafloor scenarios, they are of major focus in the previous and present studies. In previous research, typical modes of stable and peak impact forces on a suspended pipeline are identified. However, the understanding of their formation mechanism is still far from adequate. As such, the peak impact force is used in previous work to calculate drag coefficient, as it is on a more hazardous level than the stable one. The aim of this paper is to understand the formation mechanism of typical modes of impact forces; and establish a more reliable methodology to estimate the peak impact force. As such, a two-dimensional (2D) biphasic (slurry and water) numerical model is developed using ANSYS Fluent 18.0. The 2D model is then used to simulate the constant-speed submarine debris-flow impact on suspended pipelines. Based on the numerical experiments, efforts are made to provide an explanation for the underlying formation mechanism of peak impact force on a suspended pipeline due to the constant-speed submarine debris flow. Efforts are also made to set up a methodology to estimate the peak impact force on a suspended pipeline.

## 2. Model descriptions

### 2.1. General

ANSYS Fluent 18.0 is a general-purpose CFD software that includes three different Euler-Euler multiphase models: the volume of fluid (VOF) model, mixture model, and Eulerian model (Fluent, 2017). Submarine debris flow constitutes an incompressible biphasic (slurry and water) flow regime. As such, the Eulerian multiphase model is used to simulate the constant-speed submarine debris-flow impact on a suspended pipeline. In the biphasic (slurry and water) numerical model, conservation equations for mass and momentum are discretized using the Finite Volume Method (FVM). They are solved separately over the unstructured meshes for each phase. The interphase coupling is achieved through the shared pressure and interphase exchange coefficients. Hereafter, only the used aspects are stated in this section, and more detailed descriptions of the theory and associated formulations regarding Eulerian multiphase model are found in the ANSYS Fluent Theory Guide (Fluent, 2017).

### 2.2. Model domain and meshing

The geometry of computational domain is a square with dimension of $0.2*0.2\ m^2$ (Fig. 1). A pipe with outside diameter 0.01 m is placed at the centerline of domain. The centroid of pipe has a distance 0.05 m away from left boundary. As such, the pipe is located more than four times the pipe diameter away from all the boundaries, and the confining effects of computational domain on velocity fields and associated impact forces on the pipe are negligible (Zakeri et al., 2009c). The domain is discretized into unstructured meshes using Fluent Meshing module. The minimum mesh size is 4e-5 m, and the maximum is 4e-3 m. Since slurry-pipe interaction is of main interest in the study, meshes around pipe are further refined. The edge of pipe is divided into 100 uniform segments. The inflation boundary of 5 layers with growth rate 1.2 is set at the pipe edge. In total, the domain is comprised of 3830 nodes and 6868 triangular elements.

### 2.3. Boundaries and slurry properties

The inlet is on left boundary of the domain (Fig. 1). The constant velocity of slurry is assigned normal to the inlet boundary. Free pressure outlet is applied on right-side boundary. The top and bottom boundaries are set at free-slip walls. No-slip wall boundary is set at the pipe surface. Various percentages of clay (10–30%) and sand (35–55%) are used to represent 6 different concentrations of slurry (Table 1) (Zakeri et al., 2008). The inlet velocities of slurry for each concentration are set at 8 different values, i.e. 0.2, 0.4, 0.6, 0.8, 1.0, 2.0, 3.0, and 4.0 m/s. In total, 48 runs are performed in this work. Both slurry and ambient water are assumed in laminar regimes. For each run, the time step is set at 0.005 s. Each time step is iterated at most 100 times. The total running time for each run is 1.0 s. In ANSYS Fluent 18.0, both the impact force and associated impact coefficient are directly generated in output files. The impact coefficient is dimensionless impact force on a suspended pipeline. In this work, the numerical datasets of impact coefficient will be used for further analyses. According to Zakeri et al. (2008), the Reynolds number is calculated with

$$\mathrm{Re} = \frac{\rho U^2}{\tau} \tag{1}$$

where Re is the Reynolds number, $\rho$ is the density of slurry, $U$ is the velocity of slurry, and $\tau$ is the shear stress, which is calculated using the Herschel-Bulkley rheological model

$$\tau = \tau_y + K\gamma^n \tag{2}$$

where $\tau_y$ is the yield stress, $K$ is the flow consistency index, $n$ is the flow behavior index, and $\gamma$ is the shear rate. The shear rate is defined as

$$\gamma = \frac{U}{D} \tag{3}$$

where $D$ is the diameter of pipe.

## 3. Results and analyses

### 3.1. Interactions between submarine debris flow and suspended pipeline

A total of 48 runs are performed to simulate the submarine debris-flow impact on a suspended pipeline. The maximum shear rate is 400 $s^{-1}$, and Reynolds number is up to 847.8. For a real submarine debris flow, its density could be up to 1800 $kg/m^3$, and velocity is estimated to

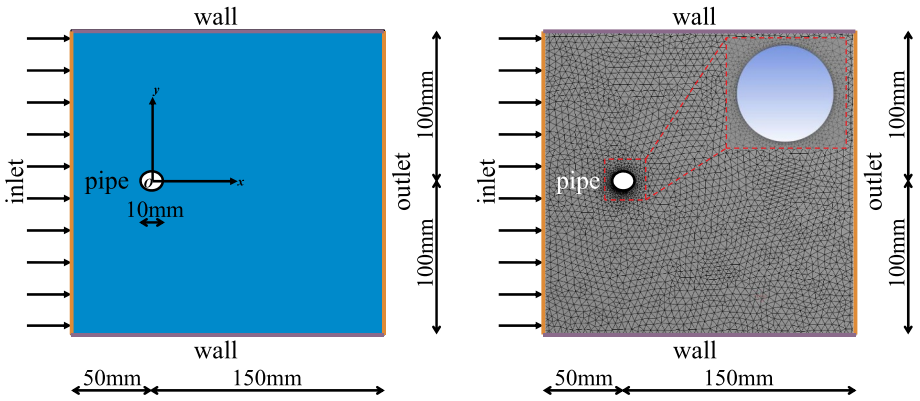


**Fig. 1.** Model domain and mesh with 6868 triangular elements.

**Table 1**
Slurry properties modified from Zakeri et al. (2008).

| Slurry | Percentage by mass (%) | | | Density (kg/m$^3$) | Herschel-Bulkley |
|---|---|---|---|---|---|
| | Clay | Water | Sand | | |
| 10%clay | 10 | 35 | 55 | 1681.0 | $\tau = 7.3 + 3.0\gamma^{0.35}$ |
| 15%clay | 15 | 35 | 50 | 1685.7 | $\tau = 20.5 + 5.5\gamma^{0.35}$ |
| 20%clay | 20 | 35 | 45 | 1687.7 | $\tau = 43.0 + 10.0\gamma^{0.35}$ |
| 25%clay | 25 | 35 | 40 | 1689.6 | $\tau = 85.0 + 12.0\gamma^{0.40}$ |
| 30%clay | 30 | 35 | 35 | 1691.6 | $\tau = 110.0 + 15.0\gamma^{0.45}$ |
| 35%clay | 35 | 35 | 30 | 1694.0 | $\tau = 161.0 + 25.0\gamma^{0.40}$ |

reach 30 m/s (Drago, 2002). The diameter of a pipe typically ranges from 0.1 to 1.0 m (Zakeri et al., 2008). Thus, the maximum shear rate could be 300 $s^{-1}$. Assuming a debris flow possesses the shear stress of 2.0 kPa (Zakeri et al., 2008), the maximum Reynolds number is calculated to be 810. Both the maximum shear rate and Reynolds number of a real submarine debris-flow impact on a suspended pipeline are covered by the 48 numerical runs, thus are considered suitable for application to field scenarios.

Mesh sensitivity analysis is carried out to evaluate the influence of mesh size on numerical results. The mesh size is reduced to a minimum of 3e-5 m and maximum of 3e-3 m. The refined domain has a total of 5986 nodes and 11104 triangular elements. A trial simulation with 15% clay content and 4.0 m/s inlet velocity is carried out. The calculated impact coefficient on the suspended pipeline is very close to that before mesh refinement (Fig. 2). As such, the numerical results are insensitive to mesh systems generated in this work, and the coarser mesh is used for the simulations.

To demonstrate the interactions between submarine debris flow and suspended pipeline, modeling results of volume fractions and velocity fields from two representative runs are shown (Fig. 3). These two runs have the same clay content of 15%, and inlet velocities of 0.2 and 1.0 m/s. It is shown that, a channel filling with water is formed behind suspended pipe. However, the entrapped water fades away as the channel becomes narrow. At inlet velocity of 0.2 m/s, the Reynolds number of flow field is calculated to be 1.9. The velocity field is symmetrical. However, when it is set at 1.0 m/s, the Reynolds number increases to be 35.1. The flow field is still symmetrical, but with eddies recirculating at the rear of the pipe. These phenomena are consistent with previous laboratory (Zakeri et al., 2008) and numerical (e.g. Fan et al., 2018; Nian et al., 2018; Guo et al., 2019) observations. In addition, the fully developed velocity fields also demonstrate that, the confining effects of selected computational domain on impact forces exerted on the pipe are negligible.

### 3.2. Modes of impact coefficients and underlying mechanism

The time-series impact coefficients imposed by slurries of different

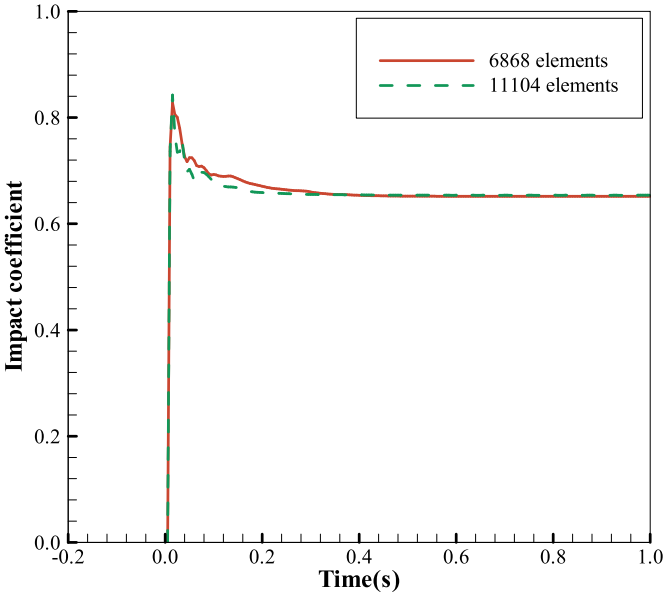


**Fig. 2.** Mesh sensitivity analysis.

clay concentrations are shown (Fig. 4). The impact coefficients are non-dimensional impact forces. The corresponding Reynolds number is also calculated for each case. Two typical modes of impact coefficients, i.e. peak and stable, acting on a suspended pipeline are observed. When the Reynolds number is high, the impact coefficient sharply rises to a peak upon initial impact, and afterwards gradually declines until it reaches a stable value. The peak impact coefficient is larger than the stable one. For the low Reynolds number, the impact coefficient gradually increases to a stable value, which means that the peak and stable impact coefficients equal each other. A critical Reynolds number is observed distinguishing the modes of impact coefficient. In present work, this critical Reynolds number seems to settle around 50.

The formation mechanism of such modes of impact force is explained as follows: According to Morison equation (Morison et al., 1950), the total impact force applied on a suspended pipeline consists of two components, i.e. velocity-related drag force and acceleration-induced inertia force.

$$F = \frac{1}{2}C_D\rho DU^2 + \frac{\pi}{4}C_M\rho D^2 a \tag{4}$$

where $F$ is the total impact force, $C_D$ is the drag coefficient, $C_M$ is the inertia coefficient, and $a$ is the acceleration.

The material acceleration of slurry is decomposed into two parts, i.e. the convective and local accelerations. The convective acceleration is

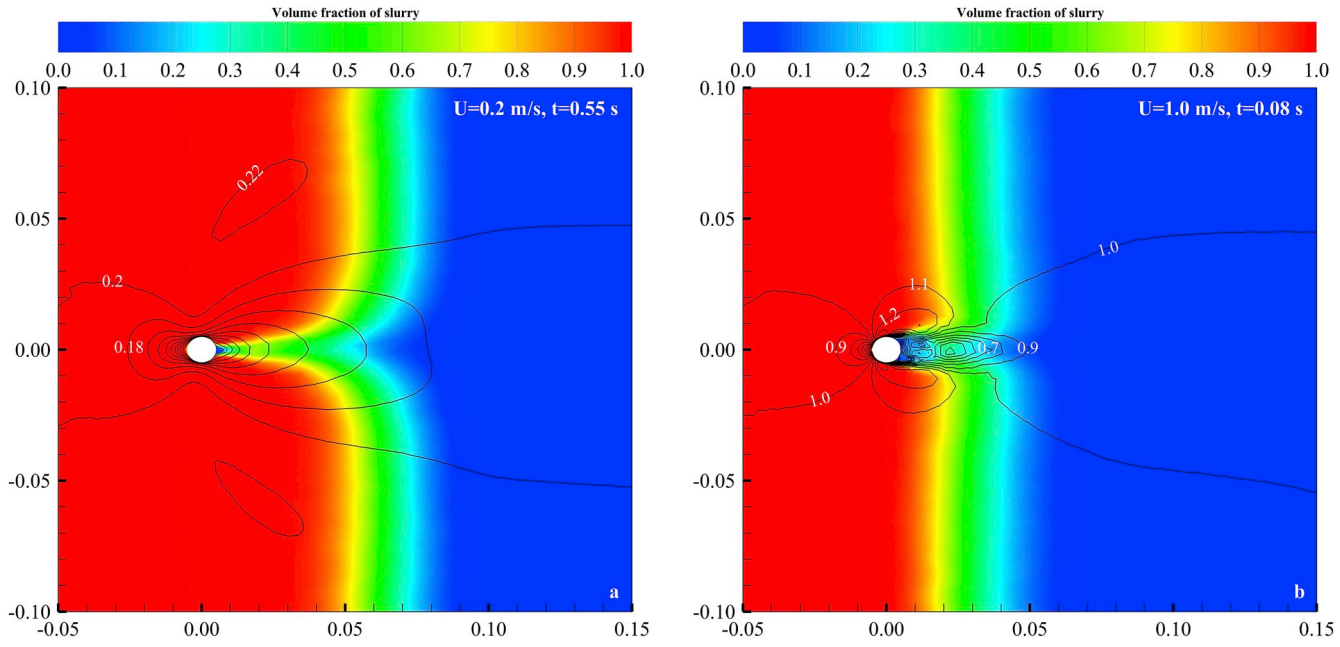


**Fig. 3.** Interactions between 15% clay slurry and suspended pipeline at two impact velocities: (a) 0.2 m/s, and (b) 1.0 m/s.

defined as the rate of change of velocity due to change of position, while the local acceleration is the rate of change of velocity with respect to time at a given point, which can be seen in the following equation

$$\frac{D\vec{u}}{Dt}=\frac{\partial\vec{u}}{\partial t}+\vec{u}\cdot\nabla\vec{u} \tag{5}$$

where $\vec{u}$ is the vectorized velocity of slurry, and $t$ is the time.

The interaction processes between slurry and pipeline can be divided into two stages, i.e. the initial and embedded impacts. The criteria used to distinguish these two stages is that, whether the pipeline is fully engulfed by slurry. Since slurry is set at constant speed, the convective acceleration is always nil. Then, at embedded impact, the acceleration-induced inertia force is zero. The total impact force merely depends on velocity-induced drag force, which sets to a stable value when imposed by a constant-speed slurry. However, at initial impact, the magnitude of slurry velocity at the position of pipeline increases from zero to constant speed within a short duration. This leads to a transient local acceleration accompanying by an immediate inertia force acting on the pipe. Superposed by velocity-induced drag force and local acceleration-induced inertia force, the total impact force presents a sharp and temporary peak at initial impact.

Note that, the inertia force will be prominent only when the Reynolds number is high enough. This is because, when it is small, the duration of initial impact will be significantly increased. Thus, the local acceleration will be greatly reduced, which inhibits the development of inertia force applied on the pipeline. When the Reynolds number is small enough, the contribution of inertia force to total impact force is negligible, and it will only be controlled by constant speed of slurry.

### 3.3. Comparison with laboratory experiment from Zakeri et al. (2008)

The peak and stable impact coefficients associated with Reynolds number for each run are listed (Table 2). As shown in Fig. 5, comparisons of impact coefficients are made between the present numerical datasets and flume experimental data collected by Zakeri et al. (2008). It is shown that, the numerical datasets generally fit the experiment results. However, when zoomed in, some differences are observed. When Reynolds number is low, the inertia forces are negligible, thus the peak and stable impact coefficients nearly overlap with each other. The peak and stable impact coefficients are slightly larger than those from Zakeri et al. (2008). This may be possible occurrence of partial slippage on the pipe surface in the laboratory experiments, whereas in the numerical model, the boundary condition of no slip wall is set. With the increase of Reynolds number, the peak impact coefficients gradually overpass the stable values. This is due to the inertia forces on the pipeline induced by local accelerations. In addition, it is observed that, the laboratory measured impact coefficients are larger than the peak impact coefficients output from the numerical model. This is possibly due to that, the downslope propagating slurries in Zakeri et al. (2008) flume experiments may possess some nonnegligible convective acceleration when impacting on a pipeline. As such, the local acceleration at initial impact on a pipeline combined with the convective acceleration of slurry contributes to enlarged magnitudes of inertia force.

### 3.4. Estimation of peak impact force

Due to inadequate understanding of formation mechanism of peak impact force, previous researchers (Fan et al., 2018; Nian et al., 2018; Guo et al., 2019) usually formulate the peak and stable impact forces on a suspended pipeline separately, and correlate them only with the impact velocity of submarine debris flow. In this work, a single formula, with combination of drag and inertia forces into a framework, is proposed to predict the peak impact force. The stable impact coefficient is affected only by the speed of submarine debris flow, and thus equals to the drag coefficient. The peak impact force per unit length on a pipeline is

$$F=F_D+F_I \tag{6}$$

where the peak impact force $F=\frac{1}{2}C_P\rho DU^2$, drag force $F_D=\frac{1}{2}C_S\rho DU^2$, and inertia force $F_I=\frac{\pi}{4}C_M\rho D^2a$, then

$$\frac{1}{2}\rho DU^2(C_P-C_S)=\frac{\pi}{4}C_M\rho D^2a \tag{7}$$

where $C_S$ and $C_P$ are the stable and peak impact coefficients. The time-averaged acceleration will be used to characterize the local acceleration at initial impact

$$\overline{a}=\frac{U-0}{\Delta t} \tag{8}$$

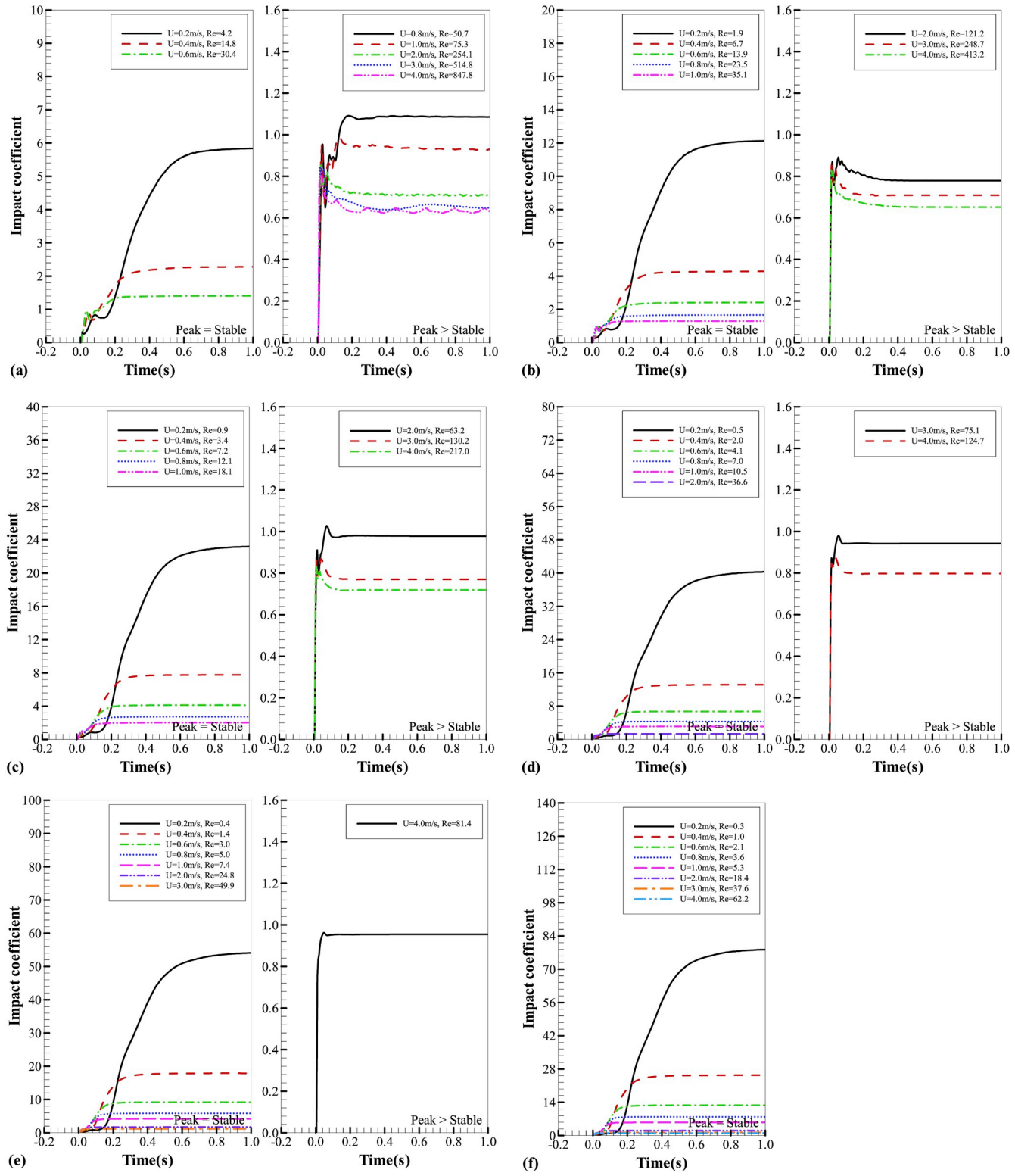


**Fig. 4.** Impact coefficients on a suspended pipeline imposed by slurries of different clay contents: (a) 10%, (b) 15%, (c) 20%, (d) 25%, (e) 30%, and (f) 35%.

where $\bar{a}$ is the time-averaged local acceleration, $\Delta t$is the time increment to reach peak impact coefficient. Then, Eq. (7) is further manipulated into

$$C_M = \frac{2}{\pi}(C_P - C_S)\gamma\Delta t \tag{9}$$

The peak and stable impact coefficients, shear rate, and duration to reach peak, are known and listed in Table 2. Then, the inertia coefficient is readily obtained. The relation between inertia coefficient and Reynolds number is shown in Fig. 6. The fitted relation for inertia coefficient is

**Table 2**
Peak and stable impact coefficients, inertia coefficients, and Reynolds number.

| slurry | Velocity(m/s) | shear rate ($s^{-1}$) | Reynolds number | peak impact coefficient | stable impact coefficient | Δt (s) | inertia coefficient |
|---|---|---|---|---|---|---|---|
| 10%clay | 0.2 | 20 | 4.2 | 5.840 | 5.840 | 1.000 | 0.000 |
| 10%clay | 0.4 | 40 | 14.8 | 2.280 | 2.280 | 1.000 | 0.000 |
| 10%clay | 0.6 | 60 | 30.4 | 1.406 | 1.406 | 1.000 | 0.000 |
| 10%clay | 0.8 | 80 | 50.7 | 1.091 | 1.085 | 0.180 | 0.055 |
| 10%clay | 1.0 | 100 | 75.3 | 0.989 | 0.930 | 0.125 | 0.470 |
| 10%clay | 2.0 | 200 | 254.1 | 0.821 | 0.706 | 0.055 | 0.806 |
| 10%clay | 3.0 | 300 | 514.8 | 0.812 | 0.647 | 0.030 | 0.946 |
| 10%clay | 4.0 | 400 | 847.8 | 0.802 | 0.624 | 0.025 | 1.134 |
| 15%clay | 0.2 | 20 | 1.9 | 12.131 | 12.131 | 1.000 | 0.000 |
| 15%clay | 0.4 | 40 | 6.7 | 4.284 | 4.284 | 1.000 | 0.000 |
| 15%clay | 0.6 | 60 | 13.9 | 2.412 | 2.412 | 1.000 | 0.000 |
| 15%clay | 0.8 | 80 | 23.5 | 1.660 | 1.660 | 1.000 | 0.000 |
| 15%clay | 1.0 | 100 | 35.1 | 1.296 | 1.296 | 1.000 | 0.000 |
| 15%clay | 2.0 | 200 | 121.2 | 0.856 | 0.779 | 0.065 | 0.638 |
| 15%clay | 3.0 | 300 | 248.7 | 0.800 | 0.709 | 0.045 | 0.782 |
| 15%clay | 4.0 | 400 | 413.2 | 0.750 | 0.652 | 0.035 | 0.874 |
| 20%clay | 0.2 | 20 | 0.9 | 23.200 | 23.200 | 1.000 | 0.000 |
| 20%clay | 0.4 | 40 | 3.4 | 7.752 | 7.752 | 1.000 | 0.000 |
| 20%clay | 0.6 | 60 | 7.2 | 4.114 | 4.114 | 1.000 | 0.000 |
| 20%clay | 0.8 | 80 | 12.1 | 2.727 | 2.727 | 1.000 | 0.000 |
| 20%clay | 1.0 | 100 | 18.1 | 2.015 | 2.015 | 1.000 | 0.000 |
| 20%clay | 2.0 | 200 | 63.2 | 1.028 | 0.978 | 0.075 | 0.478 |
| 20%clay | 3.0 | 300 | 130.2 | 0.825 | 0.770 | 0.065 | 0.683 |
| 20%clay | 4.0 | 400 | 217.0 | 0.808 | 0.719 | 0.035 | 0.794 |
| 25%clay | 0.2 | 20 | 0.5 | 40.327 | 40.327 | 1.000 | 0.000 |
| 25%clay | 0.4 | 40 | 2.0 | 13.131 | 13.131 | 1.000 | 0.000 |
| 25%clay | 0.6 | 60 | 4.1 | 6.721 | 6.721 | 1.000 | 0.000 |
| 25%clay | 0.8 | 80 | 7.0 | 4.286 | 4.286 | 1.000 | 0.000 |
| 25%clay | 1.0 | 100 | 10.5 | 3.098 | 3.098 | 1.000 | 0.000 |
| 25%clay | 2.0 | 200 | 36.6 | 1.314 | 1.314 | 1.000 | 0.000 |
| 25%clay | 3.0 | 300 | 75.1 | 0.981 | 0.943 | 0.055 | 0.399 |
| 25%clay | 4.0 | 400 | 124.7 | 0.873 | 0.797 | 0.035 | 0.678 |
| 30%clay | 0.2 | 20 | 0.4 | 54.032 | 54.032 | 1.000 | 0.000 |
| 30%clay | 0.4 | 40 | 1.4 | 17.872 | 17.872 | 1.000 | 0.000 |
| 30%clay | 0.6 | 60 | 3.0 | 9.201 | 9.201 | 1.000 | 0.000 |
| 30%clay | 0.8 | 80 | 5.0 | 5.845 | 5.845 | 1.000 | 0.000 |
| 30%clay | 1.0 | 100 | 7.4 | 4.195 | 4.195 | 1.000 | 0.000 |
| 30%clay | 2.0 | 200 | 24.8 | 1.730 | 1.730 | 1.000 | 0.000 |
| 30%clay | 3.0 | 300 | 49.9 | 1.178 | 1.178 | 1.000 | 0.000 |
| 30%clay | 4.0 | 400 | 81.4 | 0.955 | 0.955 | 1.000 | 0.000 |
| 35%clay | 0.2 | 20 | 0.3 | 78.250 | 78.250 | 1.000 | 0.000 |
| 35%clay | 0.4 | 40 | 1.0 | 25.417 | 25.417 | 1.000 | 0.000 |
| 35%clay | 0.6 | 60 | 2.1 | 12.751 | 12.751 | 1.000 | 0.000 |
| 35%clay | 0.8 | 80 | 3.6 | 7.894 | 7.894 | 1.000 | 0.000 |
| 35%clay | 1.0 | 100 | 5.3 | 5.523 | 5.523 | 1.000 | 0.000 |
| 35%clay | 2.0 | 200 | 18.4 | 2.079 | 2.079 | 1.000 | 0.000 |
| 35%clay | 3.0 | 300 | 37.6 | 1.317 | 1.317 | 1.000 | 0.000 |
| 35%clay | 4.0 | 400 | 62.2 | 1.036 | 1.036 | 1.000 | 0.000 |

$$C_M = \begin{cases} 0.2975\ln(\mathrm{Re}) - 0.8533, & \mathrm{Re} \geq 17.6,\ R^2 = 0.88 \\ 0 & ,\ \mathrm{Re} < 17.6,\ R^2 = 1.00 \end{cases} \tag{10}$$

The critical Reynolds number for fitted relation is set at 17.6, which is smaller than that of the original numerical datasets (50). This resetting of critical Reynolds number is on conservative side for prediction of peak impact force. Note that, when Reynolds number is lower than this critical value, the pipeline still experiences some inertia force, as reflected from the fluctuation of impact coefficient before reaching stable. However, the peak impact force of engineering interest at lower Reynolds number is the stable impact force. Thus, it is reasonable to set the inertia coefficient at nil for low Reynolds number.

The drag coefficient is taken as the stable impact coefficient

$$C_D = 0.58 + \frac{18}{\mathrm{Re}^{0.9}}, \quad R^2 = 0.96 \tag{11}$$

Finally, the peak impact force per unit length on a pipeline is

$$F = F_D + F_I = \frac{1}{2}C_D\rho D U^2 + \frac{\pi}{4}C_M\rho D^2\overline{a} \tag{12}$$

### 3.5. Comparison with numerical datasets from Fan et al. (2018) and Nian et al. (2018)

To demonstrate the proposed relationship between inertia coefficient and Reynolds number, comparisons are made with published numerical datasets (Fan et al., 2018; Nian et al., 2018). For the calculation of inertia coefficient based on numerical datasets from Fan et al. (2018) and Nian et al. (2018), time increments are assumed as 0.025 and 0.040 s. In addition, datasets with Reynolds number lower than the critical Reynolds number 17.6 are abandoned. The available numerical datasets are listed in Tables 3 and 4. Then, comparison between the third-party numerical datasets and present relation proposed in this work is shown in Fig. 7. It is found that, although some deviation exists between available numerical datasets and present relation curve, their overall trends are similar. One reason leading to the deviation may be

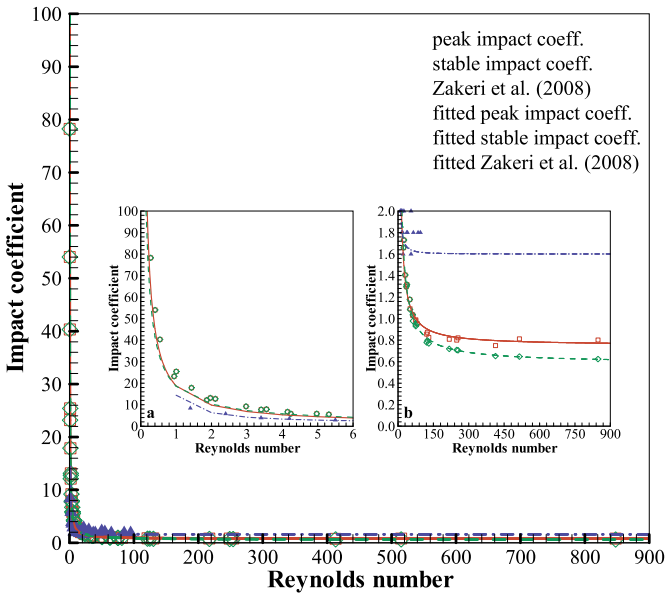


**Fig. 5.** Comparisons of impact coefficients with laboratory datasets from Zakeri et al. (2008).

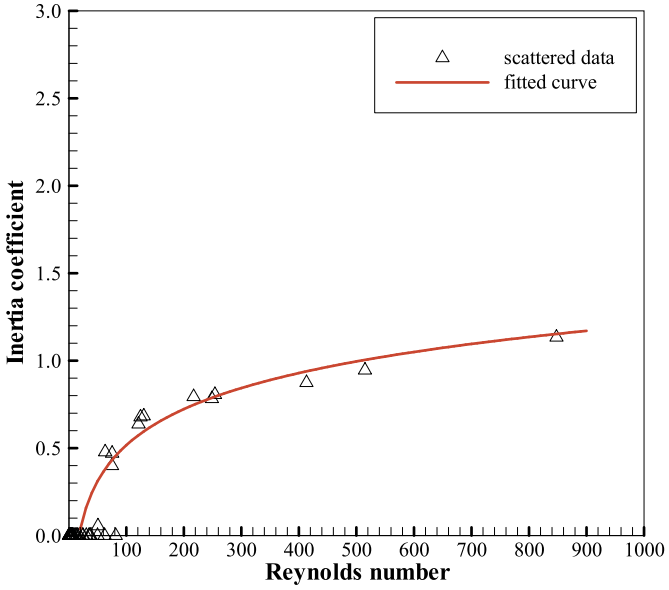


**Fig. 6.** Relation between inertia coefficient and Reynolds number.

**Table 3**
Inertia coefficients and Reynolds number modified from Fan et al. (2018).

| Reynolds number | Peak impact coefficient | Stable impact coefficient | Shear rate ($s^{-1}$) | Δt (s) | Inertia coefficient |
|---|---|---|---|---|---|
| 27.46 | 3.81 | 1.83 | 20.4 | 0.025 | 0.643 |
| 81.06 | 2.06 | 1.32 | 37.2 | 0.025 | 0.438 |
| 294.96 | 1.74 | 1.25 | 76.8 | 0.025 | 0.599 |
| 1430.59 | 1.33 | 1.06 | 188.4 | 0.025 | 0.810 |
| 10184.03 | 0.95 | 0.74 | 584 | 0.025 | 1.953 |

due to the selection of time increment as a uniform constant for all cases. The comparison with available numerical datasets provides us some confidence in the present relation. In future, lab experiments should be performed to further validate the relation.

**Table 4**
Inertia coefficients and Reynolds number modified from Nian et al. (2018).

| Reynolds number | Peak impact coefficient | Stable impact coefficient | Shear rate ($s^{-1}$) | Δt (s) | Inertia coefficient |
|---|---|---|---|---|---|
| 22.45 | 2.71 | 2.45 | 80 | 0.040 | 0.530 |
| 23.97 | 2.65 | 2.37 | 80 | 0.040 | 0.571 |
| 25.96 | 2.58 | 2.29 | 80 | 0.040 | 0.591 |
| 27.19 | 2.55 | 2.25 | 80 | 0.040 | 0.611 |
| 17.92 | 2.84 | 2.53 | 60 | 0.040 | 0.474 |
| 30.94 | 2.45 | 2.12 | 80 | 0.040 | 0.673 |
| 24.95 | 2.56 | 2.02 | 40 | 0.040 | 0.550 |
| 52.07 | 2.05 | 1.71 | 60 | 0.040 | 0.520 |
| 86.70 | 1.88 | 1.57 | 80 | 0.040 | 0.632 |
| 127.77 | 1.84 | 1.46 | 100 | 0.040 | 0.968 |
| 26.17 | 2.52 | 1.98 | 40 | 0.040 | 0.550 |
| 54.67 | 2.03 | 1.68 | 60 | 0.040 | 0.535 |
| 91.10 | 1.86 | 1.53 | 80 | 0.040 | 0.673 |
| 134.36 | 1.82 | 1.42 | 100 | 0.040 | 1.019 |
| 28.33 | 2.44 | 1.90 | 40 | 0.040 | 0.550 |
| 59.63 | 1.98 | 1.64 | 60 | 0.040 | 0.520 |
| 100.00 | 1.83 | 1.45 | 80 | 0.040 | 0.775 |
| 148.27 | 1.79 | 1.39 | 100 | 0.040 | 1.019 |
| 29.61 | 2.41 | 1.86 | 40 | 0.040 | 0.561 |
| 62.63 | 1.96 | 1.61 | 60 | 0.040 | 0.535 |
| 105.43 | 1.81 | 1.43 | 80 | 0.040 | 0.775 |
| 156.83 | 1.78 | 1.37 | 100 | 0.040 | 1.045 |
| 31.92 | 2.36 | 1.81 | 40 | 0.040 | 0.561 |
| 67.48 | 1.92 | 1.58 | 60 | 0.040 | 0.520 |
| 113.58 | 1.78 | 1.40 | 80 | 0.040 | 0.775 |
| 168.93 | 1.76 | 1.34 | 100 | 0.040 | 1.070 |
| 79.10 | 1.90 | 1.46 | 40 | 0.040 | 0.448 |
| 155.80 | 1.63 | 1.29 | 60 | 0.040 | 0.520 |
| 246.30 | 1.57 | 1.24 | 80 | 0.040 | 0.673 |
| 346.47 | 1.57 | 1.20 | 100 | 0.040 | 0.943 |
| 84.78 | 1.87 | 1.44 | 40 | 0.040 | 0.438 |
| 166.07 | 1.62 | 1.28 | 60 | 0.040 | 0.520 |
| 261.41 | 1.55 | 1.22 | 80 | 0.040 | 0.673 |
| 366.46 | 1.55 | 1.20 | 100 | 0.040 | 0.892 |
| 90.48 | 1.85 | 1.41 | 40 | 0.040 | 0.448 |
| 176.33 | 1.60 | 1.27 | 60 | 0.040 | 0.504 |
| 276.49 | 1.54 | 1.21 | 80 | 0.040 | 0.673 |
| 386.41 | 1.54 | 1.20 | 100 | 0.040 | 0.866 |
| 92.88 | 1.84 | 1.40 | 40 | 0.040 | 0.448 |
| 181.04 | 1.60 | 1.26 | 60 | 0.040 | 0.520 |
| 283.89 | 1.53 | 1.21 | 80 | 0.040 | 0.652 |
| 396.79 | 1.54 | 1.20 | 100 | 0.040 | 0.866 |
| 95.81 | 1.83 | 1.41 | 40 | 0.040 | 0.428 |
| 186.91 | 1.59 | 1.25 | 60 | 0.040 | 0.520 |
| 293.28 | 1.52 | 1.28 | 80 | 0.040 | 0.489 |
| 410.12 | 1.53 | 1.20 | 100 | 0.040 | 0.841 |

## 4. Example of peak impact force estimation

A prototype scenario of submarine debris-flow impact on a submarine pipeline is proposed. In this example, a suspended pipeline with a 0.25 m diameter is installed. A submarine debris flow impinges on the suspended pipeline at 10 different constant velocities, i.e. 0.2, 0.4, 0.6, 0.8, 1.0, 2.0, 3.0, 4.0, 5.0, and 6.0 m/s. The time increment to reach peak impact force is assumed to be 0.025 s for cases with Reynolds number larger than 17.6. The debris flow has a density of 1500 $kg/m^3$. The debris flow is assumed as a Herschel-Bulkley fluid. The yield stress is 450 Pa, flow consistency index is 20 $Pa{\cdot}S^{0.35}$, and flow behavior index is 0.35.

For the purpose of method comparison, the peak impact force exerted by a submarine debris flow on a suspended pipeline per unit length is estimated with the following two approaches:

Approach I (Zakeri et al., 2008, 2009c):

$$F = \frac{1}{2} C_D \rho D U^2$$
$$C_D = 1.4 + \frac{17.5}{\mathrm{Re}^{1.25}} \tag{13}$$

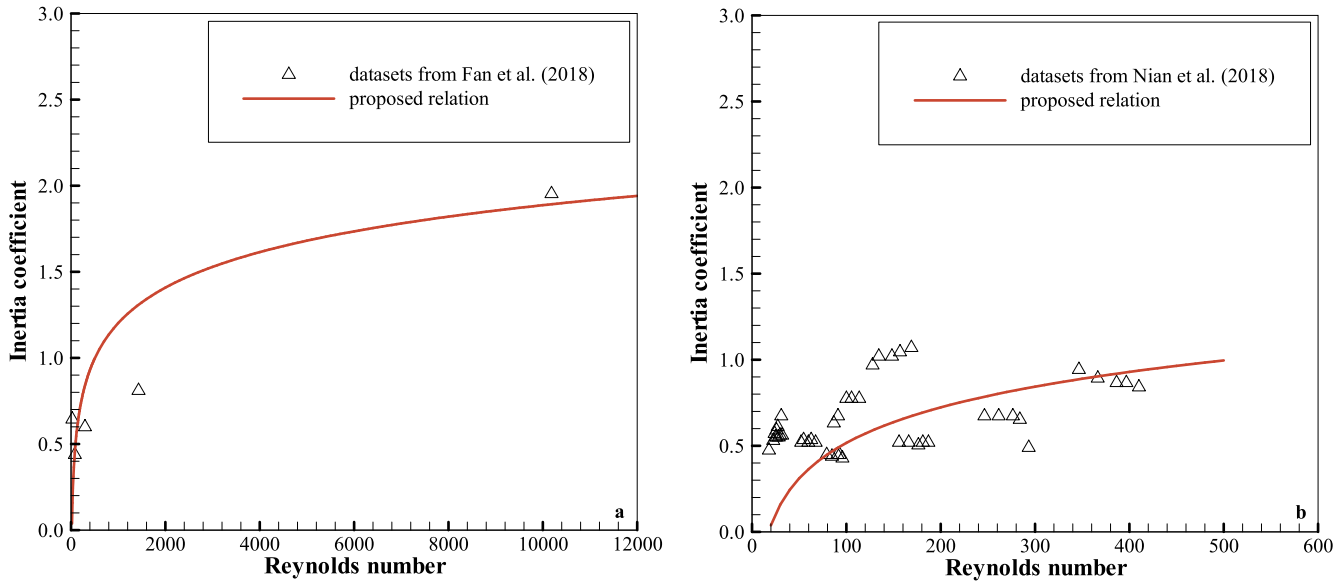


**Fig. 7.** Comparisons of relation between inertia coefficient and Reynolds number with numerical datasets from: (a) Fan et al. (2018) and (b) Nian et al. (2018).

Approach II:

$$F = \frac{1}{2}C_D\rho DU^2 + \frac{\pi}{4}C_M\rho D^2\overline{a}C_D = 0.58 + \frac{18}{\mathrm{Re}^{0.9}},\quad C_M = \begin{cases} 0.2975\ln(\mathrm{Re}) - 0.8533, & \mathrm{Re} \geq 17.6 \\ 0 & \mathrm{Re} < 17.6 \end{cases} \tag{14}$$

Table 5 is a summary of peak impact force predicted using different methods. The results are also visualized (Fig. 8). It is shown that, for low velocity impact scenarios, i.e. low Reynolds number, predictions of peak impact force with the two approaches are close to each other. This is due to that, at low Reynolds number, drag force is predominant, and the effect of inertia force is negligible. However, as Reynolds number of submarine debris flow increases, the predicted peak impact force by approach I is significantly underestimated. This is because of absence of inertia force at larger Reynolds number in approach I. In addition, predictions of only drag force by approach II at larger Reynolds number are less than those predicted by approach I. This is because, approach I is developed based on peak impact force, while approach II with drag force only is derived from stable impact force.

## 5. Discussions

### 5.1. Will peak impact force due to separated region formed behind the pipeline?

Fan et al. (2018) observed that, at initial impact, a separated region filling with ambient water is formed behind the pipeline. Afterwards, the separated region disappears at embedded impact. They claimed that, the separated region is a main reason for the formation of peak impact force, and its disappearance accounting for the stable impact force. They argued that, due to the density difference between slurry and water, pressure difference is largest when separated region shows up. To examine their viewpoints, additional numerical runs are performed by replacing the ambient water with air. The slurry is set at 15% clay (Table 1). The same inlet velocities are assigned at the inlet of domain, i.e. 0.2, 0.4, 0.6, 0.8, 1.0, 2.0, 3.0, and 4.0 m/s. Comparisons of transient impact coefficients are made between the scenarios of slurry-water and slurry-air runs (Fig. 9). It is found that only slight differences of impact coefficient exist between slurry-air and slurry-water runs. The density ratio between slurry and water is appropriately 1.7, while that ratio between slurry and air is about 1700. If separated region is a major contribution to its formation, the peak impact force would be much more remarkable in the slurry-air runs.

**Table 5**
Estimation of peak impact force using two different approaches.

| Velocity (m/s) | Reynolds number | Approach I | Approach II | | |
|---|---|---|---|---|---|
| | | Impact force (N) | Drag force (N) | Inertia force (N) | Impact force (N) |
| 0.2 | 0.1 | 1723.6 | 862.6 | 0.0 | 862.6 |
| 0.4 | 0.5 | 1269.8 | 1012.9 | 0.0 | 1012.9 |
| 0.6 | 1.1 | 1106.5 | 1126.1 | 0.0 | 1126.1 |
| 0.8 | 2.0 | 1051.1 | 1227.2 | 0.0 | 1227.2 |
| 1.0 | 3.1 | 1057.4 | 1324.7 | 0.0 | 1324.7 |
| 2.0 | 12.2 | 1625.1 | 1855.0 | 0.0 | 1855.0 |
| 3.0 | 27.1 | 2839.6 | 2536.5 | 1135.4 | 3671.9 |
| 4.0 | 47.7 | 4618.4 | 3405.1 | 3494.0 | 6899.1 |
| 5.0 | 74.0 | 6940.7 | 4473.2 | 6284.6 | 10757.8 |
| 6.0 | 105.7 | 9798.5 | 5746.8 | 9418.7 | 15165.5 |

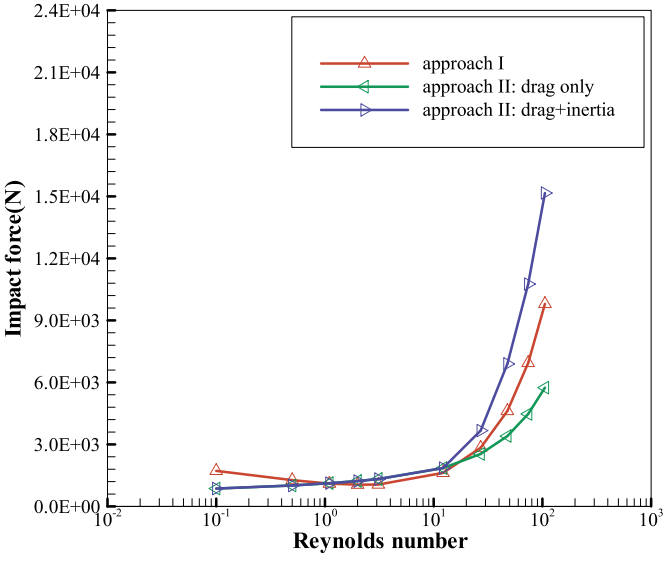


**Fig. 8.** Peak impact force predicted using different approaches.

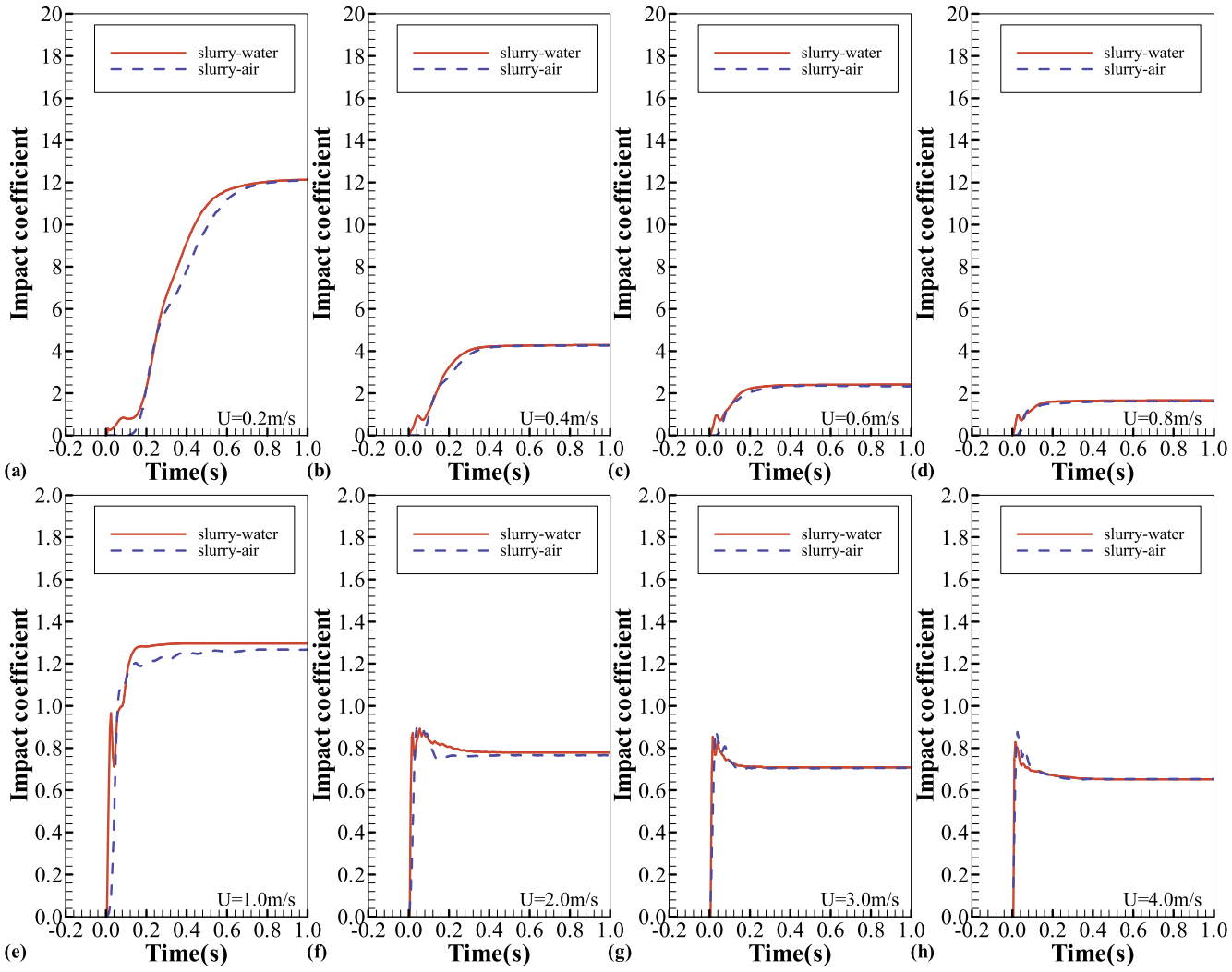


**Fig. 9.** Comparisons of impact coefficients between 15% clay content slurry-water and slurry-air runs at various impact velocities: (a) 0.2 m/s, (b) 0.4 m/s, (c) 0.6 m/s, (d) 0.8 m/s, (e) 1.0 m/s, (f) 2.0 m/s, (g) 3.0 m/s, and (h) 4.0 m/s.

### *5.2. Will peak impact force due to transition from static to kinetic friction?*

Friction is a force that resists motion when two objects are in contact. There are two forms of friction, i.e. static and kinetic. When sliding two objects past each other, the development of friction from static to kinetic is schematized (Fig. 10). The transition is briefly divided into two stages. First, the friction rapidly increases to a peak (static region); and then it presents a bluff descent to be stable (kinetic region). The static friction is always larger than kinetic one. This phenomenon of friction development plausibly resembles the mode of peak and stable impact forces acting by a constant-speed submarine debris flow on the suspended pipeline. So, will peak impact force observed in this study be a consequence of frictional transition from static to kinetic between slurry and pipe? Assuming it is true, then whatever the Reynolds number is, peak impact force at initial impact would always show up, as the friction between slurry and pipe is perpetual. However, present research reveals that, the peak impact force will only show up when Reynolds number is large enough.

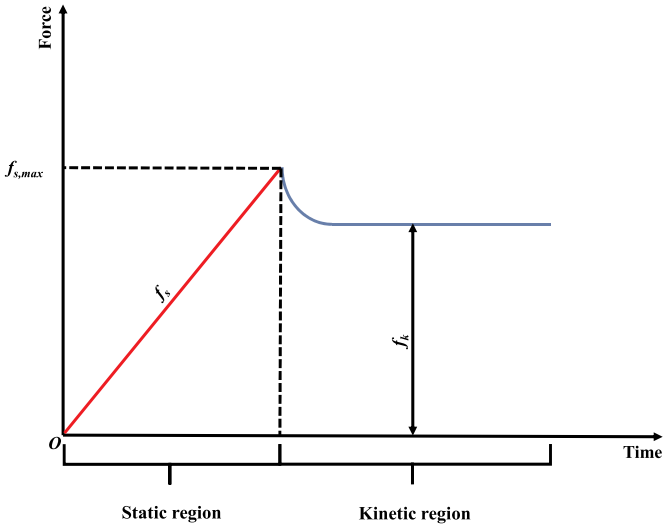


**Fig. 10.** Schematic of frictional transition from static to kinetic.

## 6. Conclusions

In this study, a 2D two-phase numerical model is developed using the ANSYS Fluent 18.0 to simulate the constant-speed submarine debris

flow impact on a suspended pipeline. Two typical modes of impact force, i.e. peak and stable, acting on the suspended pipeline are observed. The formation mechanism of peak and stable impact forces is revealed as follows. For a constant-speed submarine debris flow, its convective acceleration is nil. However, at initial impact, the suspended pipeline still experiences a short-lived local acceleration, which leads to an immediate peak before declining to be stable. The stable impact force is attributed to the speed-induced drag force, while the peak impact force is superposed by speed-induced drag force and local acceleration-induced inertia force. This temporary peak is less prominent and even negligible at lower Reynolds number, as the magnitude of local acceleration at initial impact is minor.

For the convenience of engineering application, associated formula for estimation of peak and stable impact forces are put forward. The peak impact force is the summation of drag and inertia forces, and stable impact force is only the drag force. Thus, the relation between Reynolds number and drag coefficient is developed to predict the drag force, and it is compared with the experimental datasets from Zakeri et al. (2008). The relation between Reynolds number and inertia coefficient is proposed to estimate the inertia force, and it is verified against numerical datasets available in Fan et al. (2018) and Nian et al. (2018). In this work, comparisons to existing experimental and numerical datasets provide us some confidence in the proposed relations. However, additional physical experiments are suggested to be performed to obtain more measured data for further verification and improvement of the proposed relations.

## Author contributions

**Xuesheng Qian:** Conceptualization, Methodology, Software, Validation, Formal analysis, Investigation, Data curation, Writing- Original draft, Writing- Reviewing and editing, Visualization.

**Jingping Xu:** Writing- Reviewing and editing, Resources, Supervision, Project administration, Funding acquisition.

**Yong Bai:** Resources, Supervision, Project administration, Funding acquisition.

**Himangshu S. Das:** Writing- Reviewing and editing.

## Declaration of competing interest

The authors declare that they have no known competing financial interests or personal relationships that could have appeared to influence the work reported in this paper.

## Acknowledgements

This work was supported by the Funds for International Cooperation and Exchange (Grant No. 41720104001) and National Natural Science Foundation of China; Funds for State Key Program (Grant No. 41530966) of the National Natural Science Foundation of China, and the Shenzhen Engineering Laboratory of Oil & Gas Drilling Equipment and Submarine Pipeline & Cable, China at Southern University of Science and Technology (SUSTech), China. The first author also acknowledges the postdoctoral fellowship received from SUSTech.

## References

Bea, R.G., Aurora, R.P., 1982. Design of pipelines in mudslide areas. In: Proc., Offshore Technology Conf. Offshore Technology Conference, Houston.
Demars, K.R., 1978. Design of marine pipelines for areas of unstable sediment. Transp. Eng. J. ASCE 104 (1), 109–112.
Drago, M., 2002. A coupled debris flow-turbidity current model. Ocean. Eng. 29, 1769–1780.
Dutta, S., Hawlader, B., 2019. Pipeline-soil-water interaction modeling for submarine landslide impact on suspended offshore pipelines. Géotechnique 69 (1), 29–41.
Fluent, 2017. ANSYS Fluent Theory Guide (Release 18.0). ANSYS Inc., Canonsburg, USA.
Fan, N., Nian, T., Jiao, H., Jia, Y., 2018. Interaction between submarine landslides and suspended pipelines with a streamlined contour. Mar. Georesour. Geotechnol. 36 (6), 652–662.
Guo, X., Zheng, D., Nian, T., Yin, P., 2019. Effect of different span heights on the pipeline impact forces induced by deep-sea landslides. Appl. Ocean Rea. 87, 38–46.
Kaiser, M.J., 2017. U.S. Gulf of Mexico deepwater pipeline construction-a review of lessons learned. Mar. Policy 86, 214–233.
Liu, J., Tian, J., Yi, P., 2015. Impact forces of submarine landslides on offshore pipelines. Ocean. Eng. 95, 116–127.
Li, H., Wang, L., Guo, Z., Yuan, F., 2015. Drag force of submarine landslides mudflow impacting on a suspended pipeline. Ocean. Eng. 33 (6), 10–19 (in Chinese with English abstract).
Morison, J.R., O'Brien, M.P., Johnson, J.W., Schaaf, S.A., 1950. The force exerted by surface waves on piles. Pet. Trans. AIME 189, 149–154.
Malgesini, G., Terrile, E., Zuccarino, L., Parker, E., 2018. Evaluation of debris flow impact on submarine pipelines: a methodology. In: Proc., Offshore Technology Conf. Offshore Technology Conference, Houston.
Nian, T., Guo, X., Fan, N., Jiao, H., Li, D., 2018. Impact forces of submarine landslides on suspended pipelines considering the low-temperature environment. Appl. Ocean Rea. 81, 116–125.
Pazwash, H., Robertson, J.M., 1975. Forces on bodies in Bingham fluids. J. Hydraul. Res. 13 (1), 35–55.
Perez-Gruszkiewicz, S.E., 2012. Reducing underwater slide impact forces on pipelines by streamlining. J. Waterw. Port, Coast. Ocean Eng. 138 (2), 142–148.
Randolph, M.F., Gaudin, C., Gourvenec, S.M., White, D.J., Boylan, N., Cassidy, M.J., 2011. Recent advances in offshore geotechnics for deep water oil and gas developments. Ocean. Eng. 38, 818–834.
Shcapery, R.A., Dunlap, W.A., 1978. Prediction of storm-induced sea bottom movement and platform forces. In: Proc., Offshore Technology Conf. Offshore Technology Conference, Houston.
White, D.J., Randolph, M.F., Gaudin, C., Boylan, N.P., Wang, D., Boukpeti, N., Zhu, H., Sahdi, F., 2016. The impact of submarine slides on pipelines: outcomes from the COFS-MERIWA JIP. In: Proc., Offshore Technology Conf. Offshore Technology Conference, Houston.
Wang, Z., Wang, H., Zhang, Y., 2016. CFD numerical analysis of submarine landslides impact on laid-on-seafloor pipeline. Hai Yang Xue Bao 38 (9), 110–117 (in Chinese with English abstract).
Zakeri, A., Høeg, K., Nadim, F., 2008. Submarine debris flow impact on pipelines-part I: experimental investigation. Coast. Eng. 55, 1209–1218.
Zakeri, A., 2009. Review of state-of-the-art: drag forces on submarine pipelines and piles caused by landslide or debris flow impact. J. Offshore Mech. Arct. 131, 014001.
Zakeri, A., Høeg, K., Nadim, F., 2009. Submarine debris flow impact on pipelines-part II: numerical analysis. Coast. Eng. 56, 1–10.
Zakeri, A., 2009. Submarine debris flow impact on suspended (free-span) pipelines: normal and longitudinal drag forces. Ocean. Eng. 36, 489–499.
Zakeri, A., Hawlader, B., Chi, K., 2012. Drag forces caused by submarine glide block or out-runner block impact on suspended (free-span) pipelines. Ocean. Eng. 47, 50–57.